The Aligned Orbit of the Eccentric Warm Jupiter K2-232 b

Songhu Wang,[1] Joshua N. Winn,[2] Brett C. Addison,[3] Fei Dai,[4] Malena Rice,[5] Bradford Holden,[6] Jennifer A. Burt,[7] Xian-Yu Wang,[8, 9] R. Paul Butler,[10] Steven S. Vogt,[6] and Gregory Laughlin[5]

[1]Department of Astronomy, Indiana University, Bloomington, IN 47405
[2]Department of Astrophysical Sciences, Princeton University, 4 Ivy Lane, Princeton, NJ 08544
[3]University of Southern Queensland, Centre for Astrophysics, West Street, Toowoomba, QLD 4350 Australia
[4]Division of Geological and Planetary Sciences 1200 E California Blvd, Pasadena, CA 91125
[5]Department of Astronomy, Yale University, New Haven, CT 06511
[6]UCO/Lick Observatory, Department of Astronomy and Astrophysics, University of California at Santa Cruz,Santa Cruz, CA 95064
[7]Jet Propulsion Laboratory, California Institute of Technology, 4800 Oak Grove drive, Pasadena CA 91109
[8]National Astronomical Observatories, Chinese Academy of Sciences, Beijing 100012, China
[9]University of Chinese Academy of Sciences, Beijing, 100049, China
[10] Earth and Planets Laboratory, Carnegie Institution for Science, 5241 Broad Branch Road, NW, Washington, DC 20015

ABSTRACT

Measuring the obliquity distribution of stars hosting warm Jupiters may help us to understand the formation of close-orbiting gas giants. Few such measurements have been performed due to practical difficulties in scheduling observations of the relatively infrequent and long-duration transits of warm Jupiters. Here, we report a measurement of the Rossiter-McLaughlin effect for K2-232 b, a warm Jupiter on an 11.17-day orbit with an eccentricity of 0.26. The data were obtained with the Automated Planet Finder during two separate transits. The planet's orbit appears to be well-aligned with the spin axis of the host star, with a projected spin-orbit angle of $\lambda = -11.1 \pm 6.6°$. Combined with the other available data, we find that high obliquities are almost exclusively associated with planets that either have an orbital separation greater than 10 stellar radii or orbit stars with effective temperatures hotter than 6,000 K. This pattern suggests that the obliquities of the closest-orbiting giant planets around cooler stars have been damped by tidal effects.

1. INTRODUCTION

In the Solar System, the orbits of the major planets are all aligned with the net angular momentum vector of the Solar System planets to within a few degrees, and the Sun's equator is tilted by only 6° (Souami & Souchay 2012) relative to the invariable plane. The coplanarity of the Solar System was part of the original evidence leading to the proposal that the planets formed within a flat disk surrounding the Sun (Kant 1755; de Laplace 1796).

In contrast to the picture presented by our Solar System, observations of the Rossiter–McLaughlin effect (Rossiter 1924; McLaughlin 1924) occurring during exoplanetary transits have revealed that a considerable fraction of hot Jupiters are on orbits that are misaligned with the equators of their host stars (Winn et al. 2010; Albrecht et al. 2012). The origins of large spin-orbit misalignments for hot Jupiters are still unclear. The current theoretical explanations fall into two categories:

1. High-eccentricity migration, in which dynamical interactions tilt the orbit of the planet away from its initial plane. These theories invoke phenomena such as planet-planet scattering (Rasio & Ford 1996; Ford & Rasio 2008), Lidov-Kozai cycles with
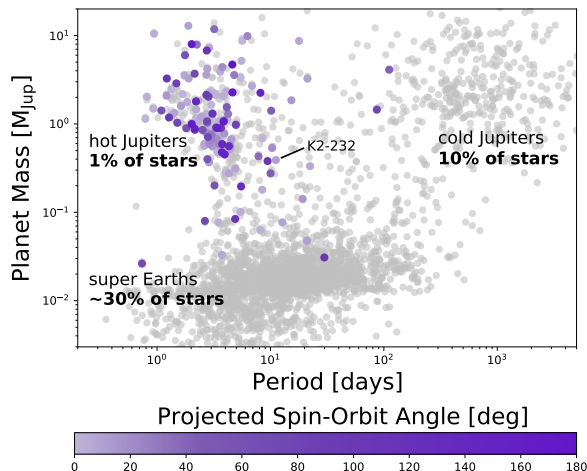
sw121@iu.edu

Figure 1. An up-to-date mass-period diagram of currently known exoplanets. Planets with Rossiter-McLaughlin (including Doppler tomography) measurements drawn from the TEPCat catalog (Southworth 2011) are shown as points color-coded by their observed spin-orbit angles, while planets without stellar obliquity measurements are depicted as gray dots. The majority of planets with existing Rossiter-McLaughlin measurements are hot Jupiters, which span a wide range of stellar obliquities. In this work, we have expanded the list of spin-orbit measurements to include a new warm Jupiter system: K2-232.

> tidal friction (Wu & Murray 2003; Fabrycky & Tremaine 2007; Naoz 2016), and secular interactions (Wu & Lithwick 2011; Petrovich 2015).

2. Obliquity excitation via mechanisms that are *unrelated* to planet migration. These include chaotic star formation (Bate et al. 2010), stochastic internal gravity waves (Rogers et al. 2012), magnetic torques between a young star and its protoplanetary disk (Lai et al. 2011), and gravitational torques from distant companions (Batygin et al. 2011; Storch et al. 2014).

Observations of "warm Jupiters" — giant planets with orbital periods longer than about 10 days — may be helpful in evaluating these formation scenarios. Unlike hot Jupiters, longer-period warm Jupiters experience relatively weak tidal interactions and can only form through high-eccentricity migration under certain conditions (Dong et al. 2013). Therefore, if high obliquities are indeed associated with high-eccentricity migration, then large spin-orbit misalignments should be confined to hot Jupiters, while warm Jupiters should have orbits that are roughly aligned with the stellar equators. If the true explanation is found in the second category of theories, spin-orbit misalignments should occur not

only in hot Jupiter systems, but also in a broader class of planetary systems, including warm Jupiters.

Furthermore, the distribution of spin-orbit angles of warm Jupiter hosts might be easier to interpret than that of hot Jupiter hosts because warm Jupiters are unlikely to have influenced the stellar rotation through tides or other proximity effects.

An effective method for measuring or placing bounds on a star's obliquity is to observe the Rossiter-McLaughlin effect, which requires spectroscopy throughout a transit. This requirement helps to explain why there are relatively few observations of the Rossiter-McLaughlin effect for warm Jupiters. Compared to hot Jupiters, the warm Jupiters have lower transit probabilities. Even for the warm Jupiters that do transit, the transits are less frequent, and the transit durations are longer. This makes it challenging to schedule transit observations from a single observatory, and it renders the observations, which require several consecutive hours of reliable data, more vulnerable to disruptions by bad weather. Therefore, while stellar obliquities of warm Jupiters may provide important clues to understand the diverse architectures of exoplanet systems, the existing measurements are sparse.

Here, we present observations of the Rossiter-McLaughlin effect for K2-232 b, a warm Jupiter of mass 0.39 $M_{\rm Jup}$ and radius 1.06 $R_{\rm Jup}$ on an 11.17-day orbit with an eccentricity of 0.26 (Brahm et al. 2018; Yu et al. 2018). In what follows, we describe our observations (§2), the parameterized model we used to determine the spin-orbit angle (§3), and the possible implications (§4).

2. OBSERVATIONS

K2-232 was observed with the Automated Planet Finder (APF) telescope (Vogt et al. 2014) on UT 29 October 2019 and UT 04 January 2020, covering two transit events of the warm Jupiter K2-232 b. Each transit was observed as a series of 20-minute exposures using the APF's $1 \times 3''$ slit, which produces a typical spectral resolution of 90,000. The APF uses the iodine-cell technique for radial-velocity determination: a container of gaseous iodine is placed in the converging beam of the telescope, imprinting the 5000–6200 Å region of the incoming stellar spectra with a dense forest of absorption lines that acts as a wavelength calibrator and provides a means of determining the spectrometer's point-spread function (PSF). The October exposures have an average of 2630 counts/pixel in the iodine region of the spectrum, while the January exposures have a lower average of 1494 counts/pixel due to a combination of clouds and worse atmospheric seeing ($1.52''$ and $1.98''$ for October and January data, respectively).
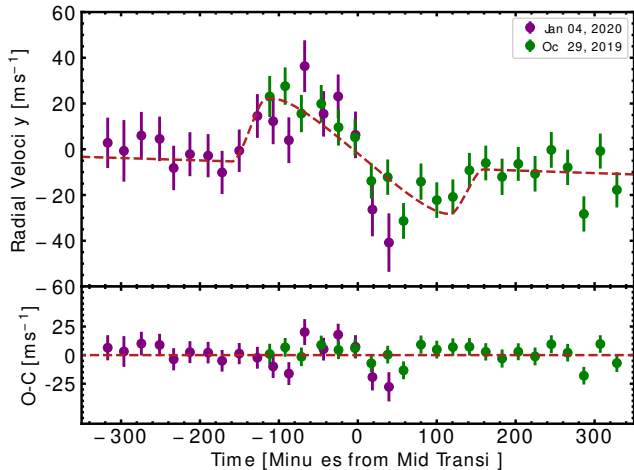
Figure 2. Spectroscopic radial velocities of K2-232 measured with the APF, as a function of orbital phase (minutes from mid-transit) along with the best-fitting Rossiter-McLaughlin model (red-dashed line). The radial velocity offsets in each of the datasets have been removed prior to fitting the combined and phased data. The green and maroon points are the radial velocities from the 29 October 2019 and 4 January 2020 transit observations, respectively. The lower panel shows the residuals between the observed data and the best-fitting model. The small structures remaining in the residuals are likely caused by stellar noise and variations in atmospheric extinction due to the presence of clouds at the end of night on 4 January 2020

.

Once the iodine region of the spectrum has been extracted, it is divided into 2 Å chunks. Each chunk is analyzed using the spectral synthesis technique originally described by Butler et al. (1996), which disentangles the stellar spectrum from the iodine absorption lines and produces an independent measure of the wavelength, instrument PSF, and Doppler shift. The Doppler velocity is calculated as the weighted mean of the velocities that are determined from each of the ≈ 700 chunks. The final internal uncertainty of each velocity is the standard deviation of the mean of all 700 chunk velocities. The October and January exposure series have mean internal uncertainties of 4.44 and 8.20 m s^{-1}, respectively. The radial velocities with uncertainties can be found in Table 1.

3. SPIN-ORBIT ANGLE DETERMINATION

We determined the sky-projected spin-orbit angle (λ) for K2-232 b using the `Allesfitter` code[1] (Günther & Daylan 2020). We simultaneously modeled the *K2* photometry of the target; the in-transit APF radial-velocity
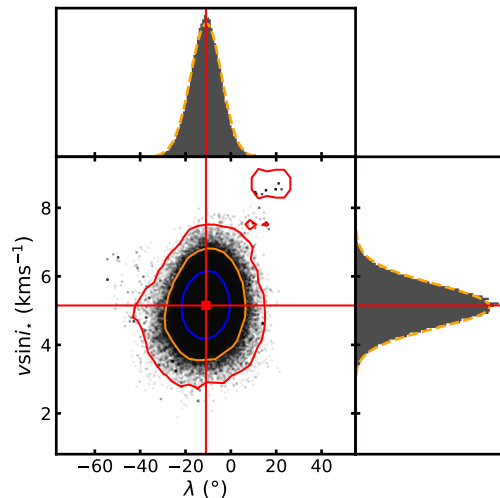
Figure 3. Posterior distributions of the projected spin-orbit angle (λ) and projected stellar rotational velocity ($v \sin i_\star$) for K2-232 from the Markov Chain Monte Carlo Rossiter-McLaughlin simulation. The posterior points inside the blue, yellow, and red contours lie within the 1σ, 2σ, and 3σ confidence regions, respectively. We have marginalized over λ and $v \sin i_\star$ and fit each with a Gaussian. The red square denotes the preferred model solution for λ and $v \sin i_\star$ as given in Table 2.

time series (which exhibit the Rossiter-McLaughlin effect); and the out-of-transit radial velocities available from the discovery papers (Yu et al. 2018; Brahm et al. 2018), taken with the APF, FEROS, CORALIE, and HARPS spectrographs.

The model parameters included the orbital period (P), time of mid-transit at a reference epoch (T_0), cosine of the orbital inclination ($\cos i$), planet-to-star radius ratio ($R_P/R_\star$), sum of radii divided by the orbital semi-major axis ($(R_\star + R_P)/a$), radial-velocity semi-amplitude (K), parameterized eccentricity and argument of periastron ($\sqrt{e} \cos \omega$, $\sqrt{e} \sin \omega$), quadratic limb darkening coefficients (q_1, q_2), sky-projected spin-orbit angle (λ), and sky-projected stellar rotational velocity ($v \sin i_\star$). Uniform priors were adopted for all of these parameters. Initial guesses for P, T_0, $\cos i$, $R_P/R_\star$, $(R_\star + R_P)/a$, K, $\sqrt{e} \cos \omega$, and $\sqrt{e} \sin \omega$ were set to the values reported by Yu et al. (2018). The initial guess for each limb darkening coefficient was 0.5. We included standard instrument offsets between radial velocities obtained from each spectrograph in the fitting. We also placed uniform priors on the additive radial velocity offsets between the time series obtained on each transit night and the radial velocities gathered outside of transit on other nights. The additive offsets account for any additional astro-
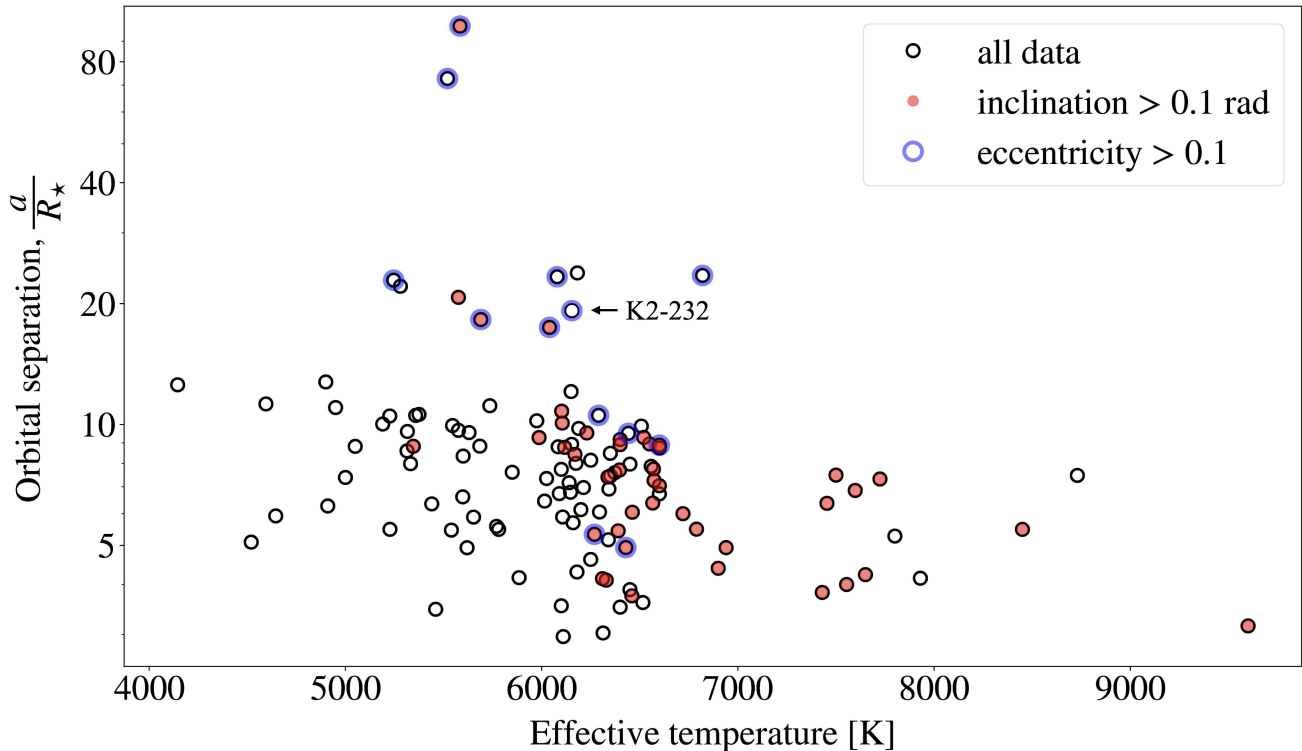
Figure 4. Key variables that may affect tidal dissipation rates, provided for all the transiting giant planets ($M_p > 0.3 M_{Jup}$) for which the Rossiter-McLaughlin effect has been reported. The horizontal axis shows effective temperature of the host star, and the vertical axis shows the dimensionless orbital separation (semimajor axis divided by stellar radius). Red points indicate the sky-projected obliquity exceeds 0.1 rad (5.7 deg), and blue encircled points indicate the orbital eccentricity exceeds 0.1, in both cases with at least 3-σ confidence. The scarcity of misaligned or eccentric systems with $a/R_\star \lesssim 10$ and $T_{eff} \lesssim 6000$ K suggests that tidal effects have damped the obliquity and eccentricity of at least some of those systems.

physical or instrumental noise on timescales longer than $\sim$ 6 hours but shorter than the total time span of all observations (2 years). These priors were bounded by reasonable intervals of ± 1000 m s^{-1}. Table 2 summarizes the model parameters, priors, and results.

We conducted three joint fits. First, we fit two separate models to independently obtain a Rossiter-McLaughlin measurement from each of the two transit events. Then, we modeled the combined dataset. Together with the in-transit data, each fit incorporated the $K2$ photometry and out-of-transit radial velocity data. For each fit, we sampled the posterior distributions of the model parameters using the Metropolis-Hastings Markov Chain Monte Carlo (MCMC) algorithm with 100 independent walkers each with 300,000 total accepted steps. The results, as listed in Table 2, provided solutions for transit and radial velocity pa-

rameters, as well as the sky-projected spin-orbit angle λ, the sky-projected stellar rotational velocity $v \sin i_\star$, and the associated 1σ uncertainties. The radial-velocity and transit parameters obtained from our analysis are in good agreement with the values from Brahm et al. (2018) and Yu et al. (2018).

The observations and the resulting best-fit model for the phased transit are shown in Figure 2, and Figure 3 shows the posterior distributions of λ and $v \sin i_\star$. Figure 3 reveals a nearly ideal 2D Gaussian distribution, suggesting that λ and $v \sin i_\star$ are not strongly correlated with each other. This is generally the case for transiting systems with moderate impact parameters ($a \cos i/R_\star \approx 0.5$) as is the case for K2-232 b (Gaudi & Winn 2007). The small fractional uncertainty in the $v \sin i_\star$ prior ($\sim 12\%$) further helps in determining λ.

We find the best-fit projected spin-orbit angle and projected stellar rotational velocity from the phased transit to be $\lambda = -11.1 \pm 6.6°$ and $v \sin i_* = 5.15 \pm 0.62$ km s^{-1}, which agree with the corresponding values from independent fits to the two transit events. Our results suggest that the orbit of K2-232 b is aligned with the spin axis of its host star.

4. DISCUSSION

Previous studies have indicated that obliquity excitation is not specific to hot Jupiters: giant planets with moderately wider orbits — wide enough to expect tidal dissipation to be insignificant — have also been observed with large orbital inclinations relative to the stellar equator. However, the number of warm Jupiters with measured spin-orbit angles is small, meaning that it is not yet clear how prevalent these large misalignments are across the longer-period giant planet population. The low obliquity of K2-232 b provides an example of a relatively well-aligned system among the longer-period giant planets. Additional observations are necessary to draw robust conclusions regarding the distribution of spin-orbit angles for warm Jupiters.

While K2-232 b is well-aligned with its host star, the planet's orbit is moderately eccentric. One might expect eccentricity and inclination to be coupled, in the sense that many interactions that would excite eccentricity would also excite inclination, and vice versa. Some examples of such interactions are planet-planet perturbations and Lidov-Kozai oscillations. Among the observations, we sometimes see orbits with high eccentricities and high inclinations, such as HD 80606 b (Winn et al. 2009b) and WASP-8 b (Queloz et al. 2010). There are also cases of low eccentricities and high inclinations, such as HAT-P-7 b (Winn et al. 2009a), CoRoT-1 b (Pont et al. 2010), and KELT-9 (Gaudi et al. 2017). And, there are cases of high eccentricities and low inclinations (at least as projected on the sky) similar to K2-232 b, such as HAT-P-2 b (Winn et al. 2007), HD 17156 b (Narita et al. 2009), and HAT-P-34 b (Albrecht et al. 2012).

The absence of a firm relationship between inclination and eccentricity is a clue that there are multiple physical processes at play, some of which are specific to eccentricity or to inclination. For examples, disk–planet interactions almost always damp inclinations, but they can result in a growth of eccentricity under the action of Lindblad resonances (Goldreich & Sari 2003). As for the reverse, some secular effects, such as nodal precession due to an external inclined perturber, can modify inclination without necessarily modifying eccentricity (Innanen et al. 1997). More measurements may be needed to delineate the relative contributions of each effect.

One pattern that is already clear is that the closest-orbiting planets ($a/R_\star \lesssim 10$) around cool stars ($T_{\rm eff} \lesssim 6,000$ K) tend to have both circular and well-aligned orbits. Figure 4 shows $a/R_\star$ versus stellar $T_{\rm eff}$ for all of the transiting giant planets for which λ has been reported based on observations of the Rossiter-McLaughlin effect. The data were drawn from the TEPCAT database[2] and restricted to cases for which the planet is more massive than Saturn ($0.3\,M_{\rm Jup}$). The blue encircled points are those systems for which Doppler observations have shown that the eccentricity exceeds 0.1 and differs from zero with at least 3-σ confidence. The red filled points are those for which Rossiter-McLaughlin observations have shown that λ exceeds 0.1 radians (5.7°) and differs from zero with at least 3-σ confidence.

Figure 4 shows a mixture of red points, blue points, red and blue points, and uncolored points, illustrating the point that eccentricity and inclination are not always observed to go together. The subject of this paper, K2-232, is represented by a blue point with $a/R_\star \approx 19$ and $T_{\rm eff} \approx 6154$ K.

Note, too, that the red and blue points are almost *all* found outside of the lower left corner. The systems with $a/R_\star \lesssim 10$ and $T_{\rm eff} \lesssim 6000$ K are not demonstrably inclined or eccentric (although in some cases the uncertainties are large). Apparently, the hottest Jupiters around relatively cool stars have lower eccentricities and inclinations than the other members of the sample. This may be evidence for tidal dissipation, which acts to dynamically cool the system. Dissipation rates are strong functions of orbital separation and may also depend sensitively on the internal structure of the star (although for eccentricity damping, tidal dissipation within the planet is expected to be at least as important the dissipation within the star).

Thus, the current dataset, limited though it might be, provides evidence that tidal dissipation has reoriented and circularized the orbits of hot Jupiters.

---

[2] https://www.astro.keele.ac.uk/jkt/tepcat/

Wang et al.

Table 1. Radial velocities for the K2-232 system collected with the APF in this work

Time (BJD)	RV ($\mathrm{m\,s^{-1}}$)	σ_{RV} ($\mathrm{m\,s^{-1}}$)
Oct. 29, 2019		
2458785.76135	54.43	6.22
2458785.77494	58.95	4.97
2458785.78924	46.95	4.93
2458785.80668	51.24	5.0
2458785.82189	40.96	4.69
2458785.83645	36.59	4.67
2458785.85075	17.47	4.15
2458785.86519	19.14	4.21
2458785.8791	0.0	4.39
2458785.89446	17.18	4.55
2458785.90838	9.12	4.32
2458785.92253	10.52	4.06
2458785.93707	22.14	4.04
2458785.95148	25.33	3.95
2458785.96582	19.29	4.56
2458785.98007	24.96	3.62
2458785.99483	20.63	4.26
2458786.00914	31.08	4.38
2458786.02352	23.42	4.19
2458786.03779	3.06	4.16
2458786.05224	30.56	4.07
2458786.06682	13.6	4.18
Jan. 4, 2020		
2458852.62955	9.26	7.32
2458852.64381	5.75	10.65
2458852.65918	12.45	6.25
2458852.67522	10.99	5.22
2458852.68760	-1.73	5.16
2458852.70191	4.28	4.99
2458852.71790	3.62	4.65
2458852.73021	-3.69	4.68
2458852.74530	5.81	4.29
2458852.76125	20.99	4.89
2458852.77514	18.67	5.77
2458852.78896	10.38	5.71
2458852.80286	42.77	7.80
2458852.81951	21.92	5.60
2458852.83234	29.54	4.96
2458852.84758	12.73	6.02
2458852.86249	-19.92	8.31
2458852.87701	-34.37	9.8

REFERENCES

Table 2. System Parameters, Priors, and Results for K2-232

Parameter	Priors[a]	Results 29 Oct. 2019	Results 4 Jan. 2020	Preferred Solution Results combined transits
Fitted Parameters:				
Orbital period, P (days)	$10; 11.168454; 12$	11.168452 ± 0.000025	11.168466 ± 0.000024	11.168455 ± 0.000023
Mid-transit epoch (2450000-BJD), T_0	7825.3^b	8305.59490 ± 0.00099	8339.1008 ± 0.0010	8339.10040 ± 0.0010
Cosine of the orbital inclination, $\cos i$	$0; 0.015; 1$	$0.0345^{+0.0028}_{-0.0024}$	$0.0344^{+0.0029}_{-0.0024}$	$0.0344^{+0.0028}_{-0.0023}$
Planet-to-star radius ratio, $R_P/R_\star$	$0; 0.08868; 1$	$0.09142^{+0.00052}_{-0.00049}$	$0.09138^{+0.00052}_{-0.00048}$	$0.09140^{+0.00051}_{-0.00048}$
Sum of radii divided by the orbital semimajor axis, $(R_\star + R_P)/a$	$0; 0.05654; 1$	$0.0676^{+0.0026}_{-0.0023}$	$0.0676^{+0.0027}_{-0.0023}$	$0.0675^{+0.0026}_{-0.0023}$
RV semi-amplitude, K (m s^{-1})	$0; 33; 1000$	32.4 ± 2.5	32.3 ± 2.6	32.4 ± 2.5
Eccentricity parameter 1, $\sqrt{e}\cos\omega$	$-1.0; -0.453; 1.0$	$-0.441^{+0.035}_{-0.030}$	$-0.440^{+0.036}_{-0.031}$	$-0.440^{+0.035}_{-0.030}$
Eccentricity parameter 2, $\sqrt{e}\sin\omega$	$-1.0; -0.231; 1.0$	$-0.217^{+0.076}_{-0.061}$	$-0.217^{+0.081}_{-0.062}$	$-0.221^{+0.074}_{-0.060}$
Limb-darkening coefficient 1, q_1	$0; 0.5; 1.0$	0.538 ± 0.068	0.544 ± 0.067	0.540 ± 0.068
Limb-darkening coefficient 2, q_2	$0; 0.5; 1.0$	$0.187^{+0.054}_{-0.043}$	$0.183^{+0.054}_{-0.041}$	$0.185^{+0.054}_{-0.043}$
Stellar rotation velocity, $v\sin i_\star$ (km s^{-1})	$0; 5; 10$	5.23 ± 0.72	$5.5^{+1.8}_{-1.6}$	5.15 ± 0.62
Projected spin-orbit angle, λ (deg)	$-180; 0; 180$	-14.5 ± 7.7	-2^{+12}_{-16}	-11.1 ± 6.6
Relative RV Offset for in-transit APF, Oct. 29 2019 (m s^{-1})	$-1000; 0; 1000$	32.0 ± 3.1	...	32.8 ± 2.8
Relative RV Offset for in-transit APF, Jan. 4 2020 (m s^{-1})	$-1000; 0; 1000$	...	8.6 ± 4.3	$7.1^{+3.2}_{-3.5}$
Relative RV Offset for out-of-transit APF (m s^{-1})	$-1000; 0; 1000$	-98.7 ± 1.9	$98.7^{+1.9}_{-1.8}$	$-98.7^{+1.9}_{-1.7}$
Relative RV Offset for Coralie (m s^{-1})	$-1000; 0; 1000$	-57^{+19}_{-22}	-57^{+19}_{-22}	-58^{+19}_{-22}
Relative RV Offset for FEROS (m s^{-1})	$-1000; 0; 1000$	3.5 ± 2.1	3.4 ± 2.1	3.5 ± 2.1
Relative RV Offset for HARPS (m s^{-1})	$-1000; 0; 1000$	-0.7 ± 2.7	$-0.6^{+2.7}_{-2.5}$	$-0.8^{+2.7}_{-2.5}$
Derived Parameters:				
Planetary radius R_b (R$_{jup}$)	...	$0.380^{+0.049}_{-0.044}$	$0.378^{+0.049}_{-0.045}$	$0.378^{+0.047}_{-0.045}$
Planetary Mass M_b (M$_{jup}$)	...	1.097 ± 0.025	1.096 ± 0.025	1.097 ± 0.024
Impact parameter b	...	0.587 ± 0.014	0.586 ± 0.013	0.587 ± 0.013
Transit duration T_{14} (h)	...	5.2893 ± 0.010	5.2893 ± 0.010	5.2895 ± 0.0099
Transit depth δ	...	0.009331 ± 0.000019	0.009330 ± 0.000018	$0.009330^{+0.000019}_{-0.000021}$
Inclination i ($^\circ$)	...	$88.02^{+0.14}_{-0.16}$	$88.03^{+0.14}_{-0.17}$	$88.03^{+0.13}_{-0.16}$
Eccentricity e	...	$0.245^{+0.020}_{-0.022}$	$0.246^{+0.020}_{-0.022}$	$0.247^{+0.020}_{-0.021}$
Argument of periastron ω (deg)	...	$206.3^{+8.0}_{-9.4}$	$206.3^{+7.8}_{-9.8}$	$206.7^{+7.8}_{-9.0}$
Limb darkening; u_1	...	$0.276^{+0.061}_{-0.053}$	$0.272^{+0.058}_{-0.052}$	$0.273^{+0.059}_{-0.053}$
Limb darkening; u_2	...	$0.461^{+0.098}_{-0.10}$	$0.468^{+0.096}_{-0.10}$	$0.464^{+0.097}_{-0.10}$

[a] The uniform priors are presented in the form of three numbers: the first number is the lower bound, the middle number is the initial guess, and the last number is the upper bound.

[b] We provided a reference mid-transit epoch for T_0. During the fit, `Allesfitter` can shift epochs to the data center to derive an optimal T_0.

Albrecht, S., Winn, J. N., Johnson, J. A., et al. 2012, ApJ, 757, 18

Bate, M. R., Lodato, G., & Pringle, J. E. 2010, MNRAS, 401, 1505

Batygin, K., Morbidelli, A., & Tsiganis, K. 2011, A&A, 533, A7

Brahm, R., Espinoza, N., Jordán, A., et al. 2018, MNRAS, 477, 2572

Butler, R. P., Marcy, G. W., Williams, E., et al. 1996, PASP, 108, 500

de Laplace, P. S. 1796, Exposition du système du monde, doi:10.3931/e-rara-497

Dong, S., Katz, B., & Socrates, A. 2013, The Astrophysical Journal Letters, 781, L5

Fabrycky, D., & Tremaine, S. 2007, ApJ, 669, 1298

Ford, E. B., & Rasio, F. A. 2008, ApJ, 686, 621

Gaudi, B. S., & Winn, J. N. 2007, ApJ, 655, 550

Gaudi, B. S., Stassun, K. G., Collins, K. A., et al. 2017, Nature, 546, 514

Goldreich, P., & Sari, R. 2003, ApJ, 585, 1024

Günther, M. N., & Daylan, T. 2020, arXiv e-prints, arXiv:2003.14371

Innanen, K. A., Zheng, J. Q., Mikkola, S., & Valtonen, M. J. 1997, AJ, 113, 1915

Kant, I. 1755, Allgemeine Naturgeschichte und Theorie des Himmels

Lai, D., Foucart, F., & Lin, D. N. C. 2011, MNRAS, 412, 2790

McLaughlin, D. 1924, The Astrophysical Journal, 60

Naoz, S. 2016, ARA&A, 54, 441

Narita, N., Hirano, T., Sato, B., et al. 2009, PASJ, 61, 991

Petrovich, C. 2015, ApJ, 799, 27

Pont, F., Endl, M., Cochran, W. D., et al. 2010, MNRAS, 402, L1

Queloz, D., Anderson, D. R., Collier Cameron, A., et al. 2010, A&A, 517, L1

Rasio, F. A., & Ford, E. B. 1996, Science, 274, 954

Rogers, T. M., Lin, D. N. C., & Lau, H. H. B. 2012, ApJL, 758, L6

Rossiter, R. 1924, The Astrophysical Journal, 60

Souami, D., & Souchay, J. 2012, A&A, 543, A133

Southworth, J. 2011, MNRAS, 417, 2166

Storch, N. I., Anderson, K. R., & Lai, D. 2014, Science, 345, 1317

Vogt, S. S., Radovan, M., Kibrick, R., et al. 2014, PASP, 126, 359

Winn, J. N., Fabrycky, D., Albrecht, S., & Johnson, J. A. 2010, ApJL, 718, L145

Winn, J. N., Johnson, J. A., Albrecht, S., et al. 2009a, ApJL, 703, L99

Winn, J. N., Johnson, J. A., Peek, K. M. G., et al. 2007, ApJL, 665, L167

Winn, J. N., Howard, A. W., Johnson, J. A., et al. 2009b, ApJ, 703, 2091

Wu, Y., & Lithwick, Y. 2011, ApJ, 735, 109

Wu, Y., & Murray, N. 2003, ApJ, 589, 605

Yu, L., Rodriguez, J. E., Eastman, J. D., et al. 2018, AJ, 156, 127